Earth and Planetary Science Letters 411 (2015) 241–252

Contents lists available at ScienceDirect

Earth and Planetary Science Letters

www.elsevier.com/locate/epsl

Distribution of the Late-Quaternary deformation in Northwestern Himalaya

R. Vassallo [a,b,*], J.-L. Mugnier [a,b], V. Vignon [c,d], M.A. Malik [e], R. Jayangondaperumal [f], P. Srivastava [f], F. Jouanne [a,b], J. Carcaillet [c,d]

[a] Université de Savoie, ISTerre, F-73376 Le Bourget du Lac, France
[b] CNRS, ISTerre, F-73376 Le Bourget du Lac, France
[c] Univ. Grenoble Alpes, ISTerre, F-38041 Grenoble, France
[d] CNRS, ISTerre, F-38041 Grenoble, France
[e] Department of Geology, University of Jammu, India
[f] Wadia Institute of Himalayan Geology, Dehra Dun, India

ARTICLE INFO

Article history:
Received 25 June 2014
Received in revised form 17 November 2014
Accepted 20 November 2014
Available online xxxx
Editor: T.M. Harrison

Keywords:
active tectonics
Himalaya
alluvial markers
quaternary geochronology
seismic hazard

ABSTRACT

Three main Cenozoic thrusts at the front of Northwestern Himalaya have accommodated most of the India–Eurasia convergence across the belt over the last million years and produced the present relief. Their recent tectonic activity is poorly known because of the long period of inaccessibility of the Jammu and Kashmir state, and because the latest and only large earthquake recorded in the region occurred in 1555 AD. We show where the deformation is localized during the Late-Quaternary, and determine shortening rates across the structures by analyzing the geometry and chronology of geomorphic markers. The Main Boundary Thrust in this region ceased moving at least ~30 ka ago. On the contrary, the more external Medlicott–Wadia Thrust and Main Frontal Thrust, both merging at depth on the sub-flat detachment of the Main Himalayan Thrust, exhibit hectometric-scale deformations accumulated during the last thousands of years. The total shortening rate absorbed by these faults over the last 14–24 ka is between 13.2 and 27.2 mm/yr (11.2 ± 3.8 and 9.0 ± 3.2 mm/yr, respectively). Part of this deformation may be associated to the geometry of the Chenab reentrant, which could generate an extra oblique component. However, the lower bound of our shortening rates is consistent with previously determined geodetic rates. Active deformation on these structures follows an in-sequence/out-of-sequence pattern, with breaking of both ramps being possible for earthquakes triggered on the main detachment.

1. Introduction

The active deformation due to the collision between India and Eurasia in the Northwestern Himalayan belt has a complex pattern in terms of structural geometry and temporal evolution (Burbank and Johnson, 1983; Powers et al., 1998). During Cenozoic times, the shortening across the belt in this region has been accommodated by a series of sub-parallel South-verging thrusts (Fig. 1A) that merge at depth on a sub-flat detachment plane, the Main Himalayan Thrust (MHT) (Srinivasan and Khar, 1996; Yin, 2006; Jouanne et al., 2011; Mugnier et al., 2013). Stress accumulating on these faults is partly released seismically, with historical events $M > 7.5$ (Ambraseys and Jackson, 2003; Ambraseys and Douglas, 2004; Hussain et al., 2009).

The last two main regional seismic events were the 1905 Kangra Mw 7.8 earthquake and the 2005 Muzaffarabad Mw 7.6 earthquake (Fig. 1A). The former, depending on the authors, occurred either beneath the frontal part of the belt or on a more internal thrust (Ni and Barazangi, 1984; Seeber and Armbruster, 1984; Bilham, 2001; Ambraseys and Douglas, 2004; Wallace et al., 2005) while the latter was clearly triggered on an internal thrust (Avouac et al., 2006; Kumahara and Nakata, 2006; Yeats et al., 2006; Kaneda et al., 2008). In between these two ruptures, a 200-km-long zone has experienced a period with no major events since 1555 AD, when the Kashmir earthquake estimated to be larger than Mw 7.5 caused damages over a vast region extending from the front of the range to the Kashmir basin (Ambraseys and Douglas, 2004). The localization of its epicenter remains unknown and so its origin cannot be assigned to any given structure.

This lack of information and the occurrence of earthquakes on internal and external structures in the region at the historical

* Corresponding author.
E-mail address: rvass@univ-savoie.fr (R. Vassallo).

http://dx.doi.org/10.1016/j.epsl.2014.11.030
0012-821X/

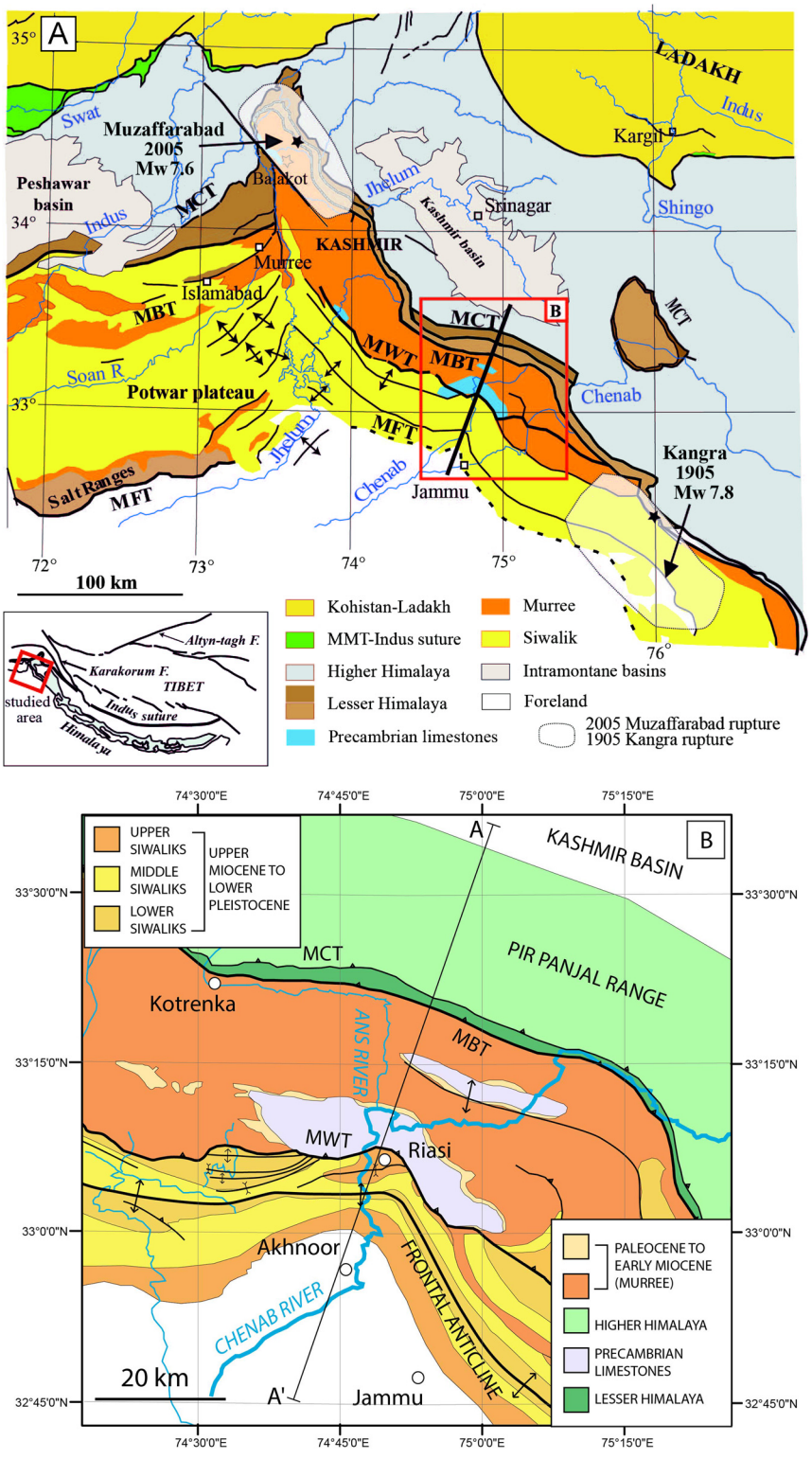

Fig. 1. A) Simplified structural map of the Northwestern Himalayan front in the Northwestern syntax region. Modified from Pêcher et al. (2008). B) Regional geological map of the study area with the principal tectonic structures: the Main Central Thrust (MCT), the Main Boundary Thrust (MBT), the Medlicott–Wadia Thrust (MWT), and the Frontal Anticline (FA) above the Main Frontal Thrust (MFT). Realized from our fieldwork data and from the geological map of Karunakaran and Rao (1979); C) Crustal cross-section of the transect indicated in B. MHT stands for the Main Himalayan Thrust and PT for the Panjal Thrust.

time-scale rise two fundamental questions about the localization of the seismogenic structures over the millennial time-scale in this part of the belt. Does deformation follow an in-sequence or an out-of-sequence pattern? And which are the most active tectonic faults capable of producing destructive earthquakes?

The present shortening across the Northwestern Himalaya is between ~12.5 and ~14 mm/yr in Kashmir/Ladakh (Schiffman et al., 2013; Jade et al., 2014) and ~13 mm/yr in northern Pakistan (Jouanne et al., 2014). Morphotectonic rates are only available 200 km to the West (Kaneda et al., 2008) and 400 km to the East

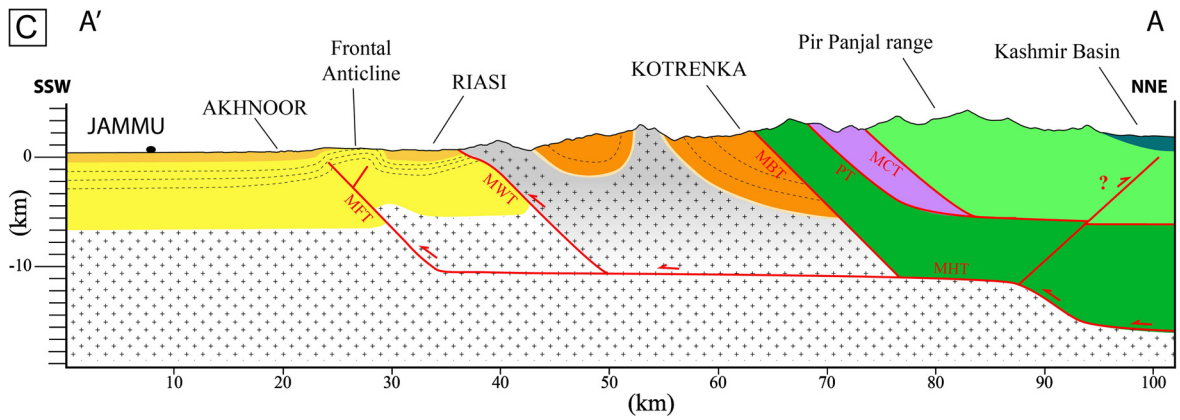

Fig. 1. (*continued*)

(Wesnousky et al., 1999) and focus on single structures that probably accommodate only a fraction of the deformation through the belt. In such a seismo-tectonic context, a crucial issue is to identify all the structures absorbing deformation within this part of the Himalaya and to quantify their shortening rates. This information will provide a better understanding of the role that each fault plays in the mountain building process and help quantifying their respective seismogenic potentials. This issue is particularly important when evaluating the seismic hazard in a densely populated region with cities of more than 1 million people like Jammu and Srinagar.

In the Northwestern Himalayan belt, three main sub-parallel South-verging thrusts are responsible for the frontal relief created during the Late Cenozoic (Nakata et al., 1991). From North to South – from the most internal to the most external fault – they are the Main Boundary Thrust (MBT) (Burbank et al., 1986), an intermediate thrust named the Medlicott–Wadia Thrust (MWT) by Thakur et al. (2010), and the Main Frontal Thrust (MFT) (Powers et al., 1998) associated to the Frontal Anticline (FA) (Fig. 1). The presence of each of these thrusts at the toes of three sub-parallel ranges shows their impact in the building and morphologic evolution of the Himalayan relief in the region of the southern active front. However, this does not mean that these sub-ranges have been built simultaneously and at the same rates.

Our aim is to determine the chronology of the tectonic activity of these thrusts and to quantify their present contribution to the accommodation of convergence. Our approach consists in studying the alluvial morphotectonic markers affected by the deformation along a transect crossing these structures. We mapped and characterized these markers using multi-spectral SPOT5 scenes and fieldwork observations. We measured their cumulated deformation across the structures using differential GPS, total station, and laser distance-meter. We dated them with *in situ* produced ^{10}Be on quartz (^{10}Be in the text, see Appendix A.1 in the Supplementary material for details), optically stimulated luminescence on quartz (OSL) and radiocarbon on organic matter (^{14}C). For each site, these geochronometers were combined taking into account the methodological constrains related to their geomorphic and sedimentological context to analyze the intrinsic methodological problems of each of them: pre-exposure ^{10}Be concentration/denudation of the surface, partial resetting/fading of the luminescence signal, organic matter remobilization. This multi-dating approach is fundamental to discuss the reliability of the ages, which have strong implications in rates estimation.

2. Morpho-structural analysis

Our study area is located on a North–South 60-km-section in the Jammu and Kashmir state, in Northwest India, between the cities of Kotrenka (North) and Akhnoor (South), passing through Riasi (Figs. 1B and 1C). The section starts at the southern front of the Pir Panjal range, where Paleozoic volcanic traps thrust a unit of quartzites of the Lesser Himalaya by means of the Panjal Thrust (PT) and the Main Central Thrust (MCT) (Fuchs, 1975; Karunakaran and Rao, 1979). These thrusts are Cenozoic structures passively transported by the more external thrusts. At the emergence of the MBT, the quartzite unit thrusts over the red sandstones of the Cenozoic Murree formation. Towards the south, the cross-section continues across the range characterized by the Jammu Limestone (Gansser, 1964), on which the Cenozoic sandstones lie unconformably. Near Riasi, the MWT allows this Precambrian stromatolites-rich carbonate to override the Late Cenozoic conglomerates and sandstones of the Siwaliks formation (Krishnaswamy et al., 1970; Hebeler et al., 2010; Vignon, 2011). The southern end of the cross-section coincides with the boundary of the Himalayan relief at the toes of the FA, which develops over the ramp of the MFT and folds the Siwaliks units with a ~20-km-wide wavelength.

The emergences at surface of the MBT and MWT are clearly visible on vertical walls of several tens of meters in the bedrock sections of different crossing valleys (Fig. 2). They are thrusts dipping northwards at 30 to 50°. Bedrock is usually fractured within zones that are around 200 m thick. Gouges zones have been identified at various places along these zones, showing that the faulting can shift or be distributed on several splays for a single thrust (Vignon, 2011). On the contrary, over several kilometers along the front of the mountain range around the Chenab river (between latitude 74°30′E and 74°49′E), we did not observe any rupture at the surface related to the MFT. We interpret it as an indication that the ramp that generated the fold is blind.

The topographic profile obtained from SRTM 30 along the cross-section reveals steps associated with the three faults. For the MBT and the MWT, these steps are determined by the long-term uplift of the respective hanging-walls, but they are accentuated by the juxtaposition of lithologies of different competences (quartzite vs sandstones and limestones vs molassic deposits, respectively). For the MFT the topography is smoother and follows the shape of the anticline with a gentler slope on the southern flank and a steeper one on the northern flank. This latter feature is consistent with the presence of a back-thrust at depth (wedge tectonics), which can be locally observed on seismic profiles (Raiverman et al., 1994).

The section between Kotrenka and Akhnoor was chosen because of the central position in the seismic gap zone, but also because of the presence of suitable geomorphic markers along the Ans and Chenab rivers and their tributaries. At each of the studied sites, well-developed Quaternary alluvial terraces and fans cross the tectonic structures (Nawani et al., 1982) and therefore record the deformation since the time of their abandonment. We used

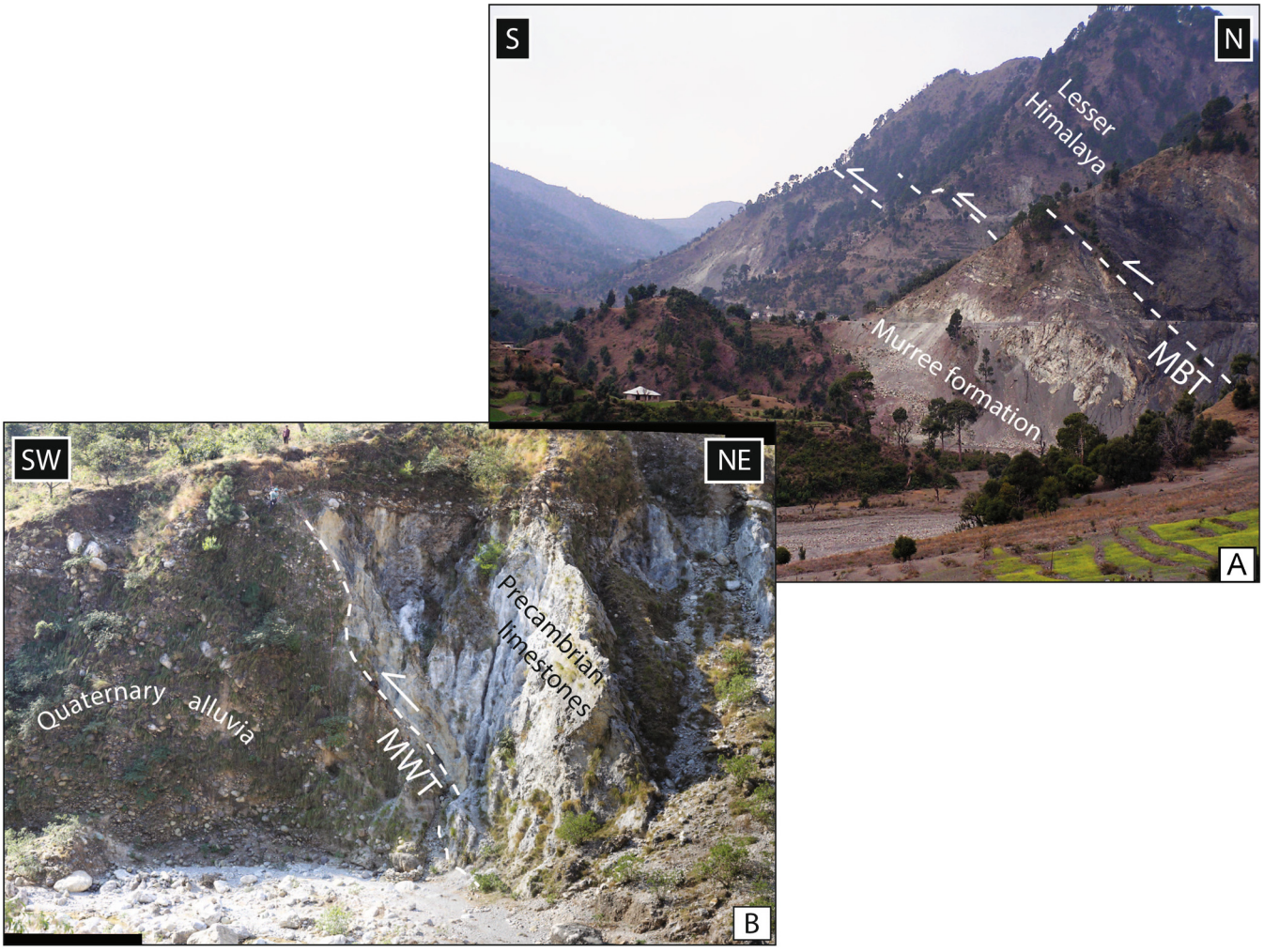

Fig. 2. Emergence at surface of the MBT (A) and MWT (B), revealed by river incision, where old formations (Lesser Himalaya series, Precambrian limestones) overthrust much younger detrital formations (Tertiary or Quaternary fluvial deposits). This implies movements of several kilometers along each of these ramps.

these morphotectonic markers to characterize and quantify the activity of the various faults. We describe the results for each site in terms of geometry, geochronology and fault slip rates.

3. The Main Boundary Thrust

In Kotrenka area, the MBT runs along the northern flank of the East–West valley of the Ans river, crossing several tributaries flowing from the North (Fig. 3A). Thick deposits of Quaternary alluvial terraces and fans are preserved on the sides of each of these tributaries and are abandoned by incisions that are locally deeper than a hundred meters. The slope of the alluvial surfaces is negatively correlated with the area of the respective catchments and varies between 6 and 10%. However, all these terraces and fans maintain a constant slope where they cross the projection at surface of the MBT. This means that the surfaces are not faulted nor folded and their ages provide a minimum bound on the most recent surface-rupturing earthquake along the MBT.

A simple altitudinal correlation of the alluvial formations is not possible in such a depositional context controlled by the catchments configuration. Therefore we sampled respectively the highest terraces and fans crossing the MBT at two different sites to date the abandonment of the oldest undeformed marker. At the outlet of the narrow North–South valley of the Ans river, before it bends 90° to the East, we dated the formation of the tread of a 200-m-wide degradational terrace, T2 (Fig. 3). At this site, where two other terraces (T1 and T3) are preserved, T2 is the only terrace that clearly crosses the MBT. This terrace, composed of meter-scale boulders and cobbles embedded in a sandy-silty matrix, has constant 6% slope (Fig. 3B). The maximum amplitude of vertical incision by the river, in its upstream part, was measured as 70 m. The flat morphology of the terrace suggests very low denudation of the surface and the boulders do not present traces of weathering nor mechanical degradation.

The dating of terrace T2 was done by using all the three geochronometers: ^{10}Be, OSL and ^{14}C. For the ^{10}Be method, we collected quartz samples from: 1) boulders well-encased in the matrix and whose tops stand between 50 and 80 cm above the flat ground; 2) quartzite cobbles at depth in a hand-dug soil pit of 1.8 m. Both the ^{10}Be distributions on boulders at surface (JK-08-19, JK-08-20 and JK-08-32) and on cobbles along the depth profile (JK-08-23 to JK-08-28) show quite large scatter (Fig. 4, Table 1). This scattering is likely due to a non-negligible ^{10}Be inherited component – acquired prior to the final deposit – that is not homogeneous for all the clasts. The samples with the relatively lowest concentrations at surface and at depth are therefore the ones with the smallest quantity of inherited ^{10}Be. Assuming no denudation, we used a least square inversion that is function of the exposure age and of the inheritance to generate a model that verifies the radionucleide production rate attenuation law of Lal (1991) taking into account these two samples with their uncertainties (JK-08-19 at surface and JK-08-25 at depth). In the concen-

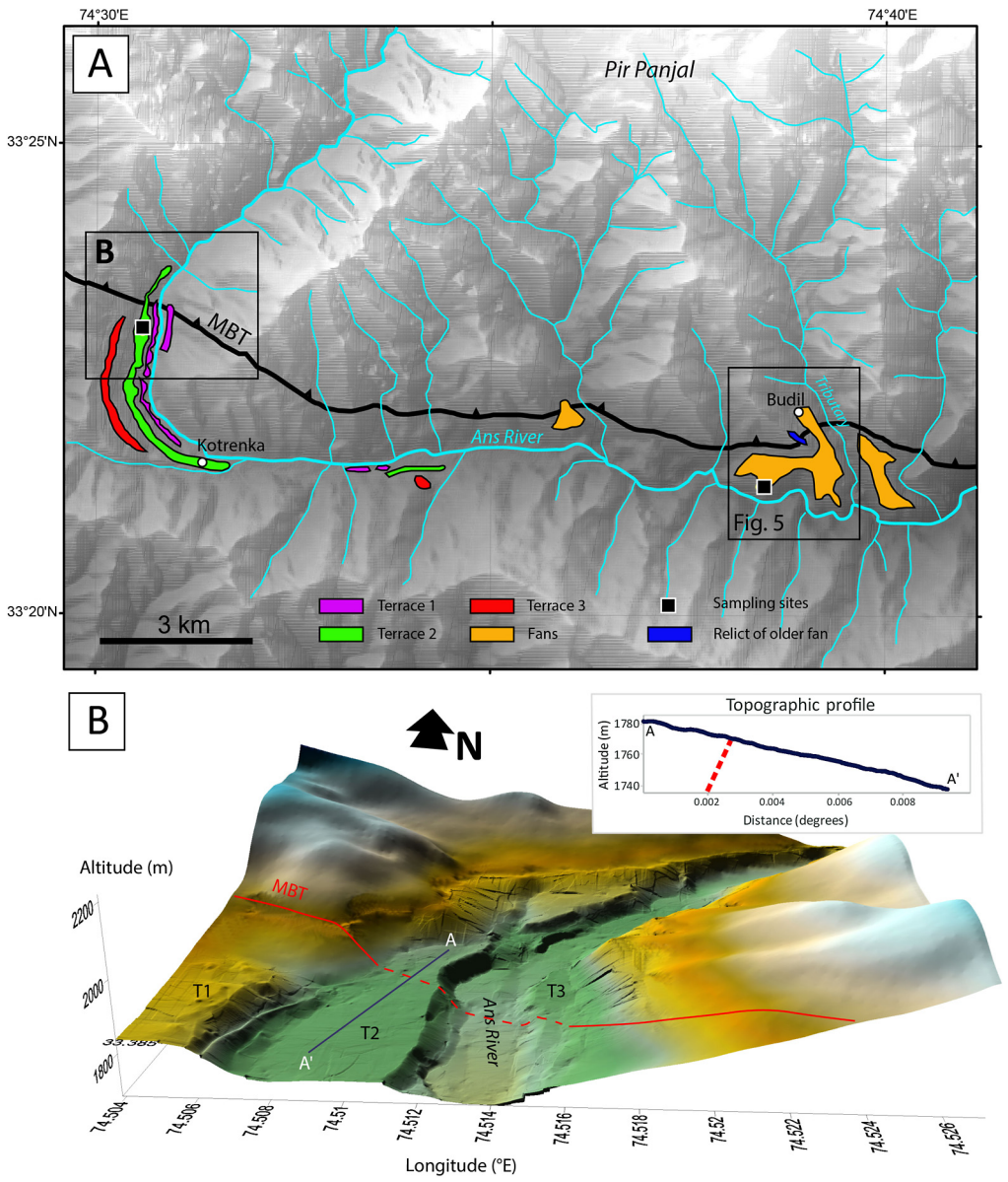

Fig. 3. A) Map of the alluvial formations along the MBT in the Ans river valley. Sampling sites for dating (^{10}Be, OSL and ^{14}C) are indicated. B) DEM of the Kotrenka site and topographic profile along terrace T2 realized from differential GPS data (for all differential GPS raw data, see Appendix A.2 in the Supplementary material). MBT does not affect the surface of the terrace, which has a constant downstream slope over more than 1 km.

tration versus depth diagram, all the other samples are situated to the right of the model, since their inherited ^{10}Be concentration is higher. Because it cannot be excluded that also these samples contain some inherited ^{10}Be, all the solutions to the left of the model are possible. The model therefore yields a maximum exposure age and a minimum inheritance value. We calculated a maximum exposure age of 5.7 ± 0.7 ^{10}Be-ka for a minimum inheritance of $21 \pm 4 \cdot 10^3$ at/g.

OSL dating of the sands contained in the soil pit, at a depth of 45 cm, gives a least (<20% of the grains) burial age of 3.8 ± 0.6 OSL-ka (JK-08-21, Table 1). For OSL analysis we prefer to use least rather than mean ages because other studies in similar geomorphic Himalayan contexts show that some sand grains are often only partially bleached, and therefore taking into account all the grains would lead to overestimate the true burial ages (Srivastava et al., 2008). This OSL age is consistent with the ^{10}Be maximum age and restricts the age of formation of the terrace to the interval 3.2–4.4 ka. ^{14}C dating on bulk organic matter contained in the paleo-soil at the same depth as the OSL sample gives an age of 4039 ± 107 cal BP (JK-08-22, Table 1), which is therefore within the OSL-^{10}Be age interval. Given the consistency of the three methods, we consider that this last result represents the most reliable and accurate age of the terrace. This means that the MBT, in this region, has not been active since at least 4 ka.

A second site near the town of Budil, 5 km to the East, is characterized by a fan that crosses the MBT perpendicularly along more than 300 m (Figs. 3A and 5A). The tread is incised by a tributary of the Ans river, with an incision reaching 160 m around the fault zone. The slope of the tread is constant (∼10%), with no scarp or inflexion at the intersection with the fault at surface (Fig. 5B). The surface of this deposit is about 200 m higher than the downstream projection of the tread of the Ans river terrace dated at 4 ka and could be interpreted as much older. However, a numerical dating is necessary to establish the exact chronology between these surfaces.

We dated the deposition of this fan by OSL and ^{14}C but could not perform a ^{10}Be sampling on this surface, entirely reworked by ploughing and anthropogenic terraces down to ∼1 m deep, in the

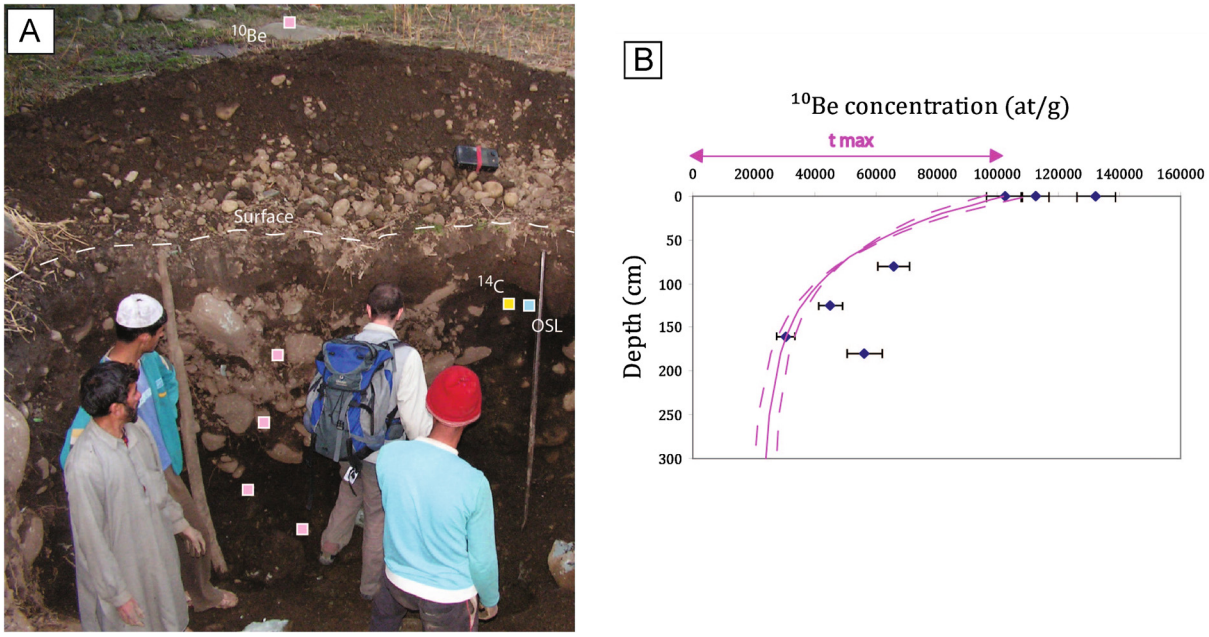

Fig. 4. A) Hand-dug soil pit within terrace T2 of Kotrenka used for ^{10}Be sampling along a depth profile, and for collecting OSL and ^{14}C samples. B) Plot of the ^{10}Be concentrations versus depth and exponential model for the maximum exposure age taking into account the samples with the least concentrations at surface and at depth (see text for explanation). For data inversion we assumed no denudation, density 2.2 g/cm^3, and particles attenuation values determined by Braucher et al. (2003). See Appendix A.1 in the Supplementary material for more details.

Table 1
Results of the ^{10}Be, OSL and ^{14}C analysis.

A) Measurements for ^{10}Be were performed at the accelerator mass spectrometry facility ASTER (Aix-en-Provence, France) after preparation of targets at the Cosmogenic Laboratory of ISTerre (Grenoble, France). Calibration against NIST Standard Reference Material 4325 with an assigned ^{10}Be/^{9}Be ratio of 2.79×10^{-11} and a ^{10}Be half-life of $1.387 \pm 0.012 \cdot 10^6$ yrs (Chmeleff et al., 2010; Korschinek et al., 2009). ^{10}Be concentration uncertainties include analytical uncertainties from the counting statistics, instrumental variability (1%) and chemical blank. Production rates were calculated with the Cronus calculator (Balco et al., 2008) using the scaling model of Lal (1991) and Stone (2000), and geomorphic shielding factors of Dunne et al. (1999). All the geochronological samples of the study area are archived in the Pangaea data repository (http://dx.doi.org/10.1594/PANGAEA.836910).

^{10}Be samples	Composition/size	Latitude	Longitude	Altitude (m)	Depth (m)	^{10}Be concentration (at/g)	Uncertainty (at/g)	Shielding factor	Surface P_0 (at/g/yr)
JK-08-32	Quartz vein in boulder	33.3860°N	74.5110°E	1790	0	1.32E+05	6.27E+03	0.9915	14.12
JK-08-19	Quartz vein in boulder	33.3860°N	74.5110°E	1790	0	1.02E+05	5.86E+03	0.9915	14.12
JK-08-20	Quartz vein in boulder	33.3860°N	74.5110°E	1790	0	1.12E+05	4.48E+03	0.9915	14.12
JK-08-28	Quartzite cobble	33.3860°N	74.5110°E	1790	0.8	6.59E+04	5.23E+03	0.9915	14.12
JK-08-26	Quartzite cobble	33.3860°N	74.5110°E	1790	1.3	4.51E+04	3.74E+03	0.9915	14.12
JK-08-25	Quartzite cobble	33.3860°N	74.5110°E	1790	1.6	3.04E+04	2.94E+03	0.9915	14.12
JK-08-23	Sandstone cobble	33.3860°N	74.5110°E	1790	1.8	5.63E+04	5.66E+03	0.9915	14.12
JK-10-60	Quartzite cobble	33.0071°N	74.7892°E	590	0	7.98E+04	6.13E+03	1	6.01
JK-10-61	Quartzite cobble	33.0071°N	74.7892°E	590	0.3	5.10E+04	7.01E+03	1	6.01
JK-10-62	Quartzite cobble	33.0071°N	74.7892°E	590	0.5	6.30E+04	5.26E+03	1	6.01
JK-10-64	Quartzite cobble	33.0071°N	74.7892°E	590	1.0	3.30E+04	3.23E+03	1	6.01
JK-10-65	Quartzite cobble	33.0071°N	74.7892°E	590	1.5	2.77E+04	4.47E+03	1	6.01

B) Measurements for OSL were performed at the Wadia Institute (Dehradun, India). SAR protocol on 30 aliquots is used to estimate mean palaeodose (Murray and Wintle, 2000). All the aliquots showing recycle ratio within 10% are considered. Water content is assumed to be 10 ± 5% by weight for all samples. Least OSL ages are obtained using the 20% of the aliquots that yield the least equivalent dose.

OSL samples	Composition	Latitude	Longitude	Altitude (m)	Depth (m)	Mean equivalent dose (Gy)	Least equivalent dose (Gy)	U (ppm)	Th (ppm)	K (%)	Cosmic rays (μGy/yr)	Dose rate (Gy/kyr)	Mean age (ka)	Least age (ka)
JK-08-21	sand	33.3860°N	74.5110°E	1790	0.45	16.0 ± 1.7	9.9 ± 1.0	2.6	8.2	0.5	150 ± 30	2.6 ± 0.3	11.1 ± 2.6	3.8 ± 0.6
JK-10-09	sand	33.3548°N	74.6410°E	1360	60	68 ± 14	52 ± 7	2.2	12.7	2.2	0	3.4 ± 0.2	20.0 ± 4.0	15.0 ± 2.0
JK-10-69	sand	33.0071°N	74.7892°E	590	6	144 ± 26	103 ± 3	3.4	20	2.3	150 ± 30	4.2 ± 0.2	34.0 ± 6.0	24.0 ± 1.0
JK-10-33	sand	33.1130°N	74.8260°E	500	55	66 ± 26	36 ± 4	1.5	7.7	1.9	0	2.7 ± 0.2	24.0 ± 10.0	14.0 ± 2.0
JK-10-80	sand	33.1120°N	74.8430°E	720	6	58 ± 7	49 ± 2	1.7	13.6	2.1	150 ± 30	3.3 ± 0.2	18.0 ± 2.0	15.0 ± 1.0

C) Measurements for ^{14}C were performed at Poznan Radiocarbon Laboratory (Poland). Calibration was obtained using the OxCal program (Ramsey, 1995).

^{14}C samples	Composition	Latitude	Longitude	Altitude (m)	Depth (m)	Not calibrated age BP (yr)	Calibrated age BP (yr)
JK-08-22	peat	33.3860°N	74.5110°E	1790	0.45	3645 ± 35	4039 ± 107
JK-10-07	charcoals	33.3548°N	74.6410°E	1360	60	$33\,990 \pm 440$	$36\,993 \pm 1364$
JK-10-08	charcoals	33.3548°N	74.6410°E	1360	60	$31\,190 \pm 330$	$33\,791 \pm 721$

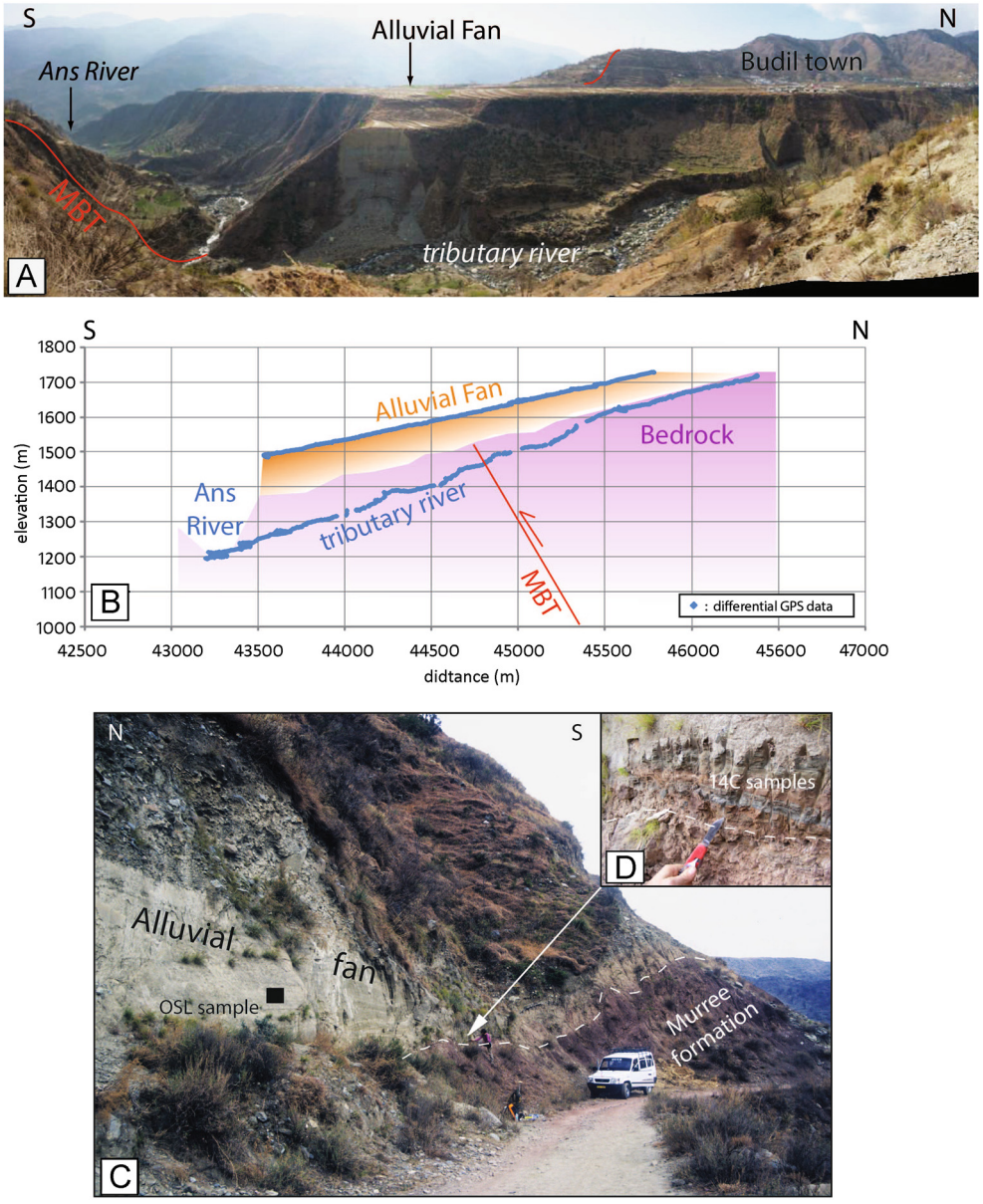

Fig. 5. A) Photograph of the Budil fan crossing the MBT in a tributary valley of the Ans river; B) Topographic profiles obtained by differential GPS of the alluvial deposits and tributary river showing no deformation of these markers across the MBT; C) Photograph of the OSL and ^{14}C sampling site at the base of the fan deposit; D) Detail of the sampling of charcoal at the very base of the fan for ^{14}C dating.

absence of large boulders. At the base of the frontal part of the fan, on a vertical section created by the recent excavation of a track, we exploited an outcrop at the contact with the Murree sandstones of the bedrock (Figs. 5C and 5D). At this site, the stratigraphy of the fan alternates coarse sand layers with silty layers containing charcoal pieces. We sampled a well-sorted silty layer, because it is likely that finer sediments have been fully bleached during transport for OSL analysis, and charcoal pieces for ^{14}C dating of the organic matter. OSL analysis on sample JK-10-09 gives a least burial age of 15.0 ± 2.0 ka and a mean burial age of 20.0 ± 4.0 ka, while ^{14}C on two charcoal samples gives two ages of $37\,000 \pm 1400$ cal BP (JK-10-07) and 33800 ± 800 cal BP (JK-10-08), respectively (Table 1). The discrepancy between the two methods implies the occurrence of a bias in the dating of the deposit for one of them. Either OSL is true and the ^{14}C ages issued from remobilization of old organic matter in this deposit, or ^{14}C could be true and OSL sample is affected by a problem of fading that underestimates the burial age. Since we have two ^{14}C similar dates, an age of ~35 ka for the base of the fan seems more likely. Considering that the younger of these two samples should be less remobilized and thus closer to the true age of deposit, and the fact that this age represents a maximum for the abandonment of the fan since it is situated at its base, these results imply that the activity of the MBT ceased at least ~30 ka ago. This is a minimum age given by the oldest marker in direct relationship with the fault, but the time of tectonic abandonment of the MBT could be much older. Consequently, even considering very long recurrence times of earthquakes on this segment of the MBT, we deduce that this fault is no longer active in our study area.

4. The Medlicott–Wadia Thrust

The MWT has a regional direction of N120°E. In the Riasi region, where the Chenab river crosses it, this structure presents a reentrant geometry (Fig. 6). At this site, cumulated reverse displacements on MWT offset a Quaternary alluvial fan creating a

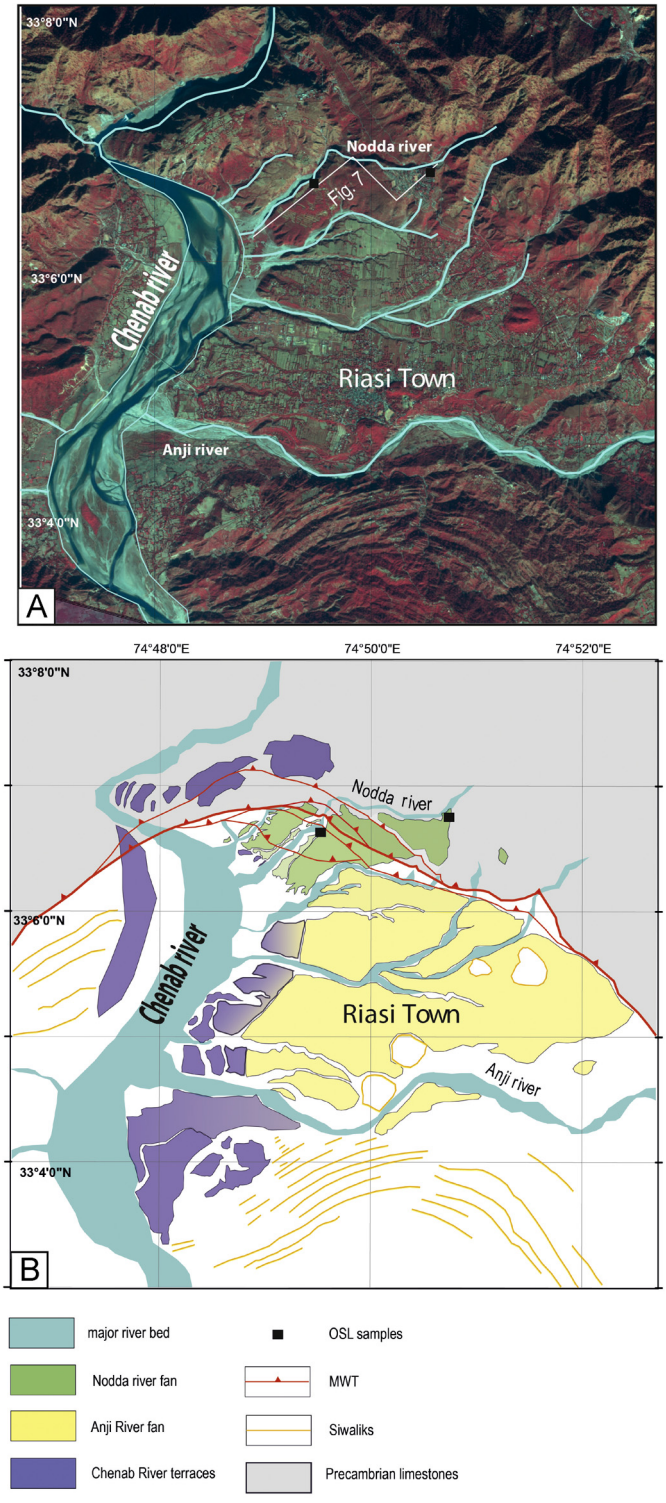

Fig. 6. A) SPOT5 image of the Riasi region showing the alluvial surfaces affected by the MWT. The location of the cross-section of Fig. 7 and of the OSL samples are indicated; B) Corresponding map of the alluvial surfaces and of the fault segments of the MWT.

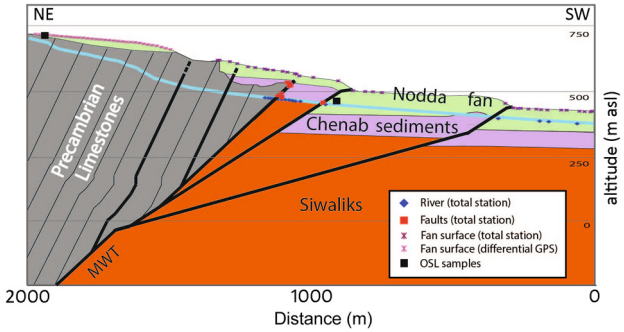

Fig. 7. Cross-section of the hectometric-scale scarp produced by the cumulated reverse movement of the different splays of the MWT in the alluvial fan of the Nodda river. Topographic and structural data were acquired by differential GPS and Total Station. The whole vertical movement across the fault zone is 150 ± 30 m. The average dip of the fault splays is 45°.

complex tectonic scarp across a fault zone 1.2 km thick. It is a hectometer-scale folding comparable with the pattern described by Kaneda et al. (2008) in the hanging wall of the Balakot–Bagh thrust at Nisar camp near Muzaffarabad, Pakistan. This scarp has an average NW–SE direction and derives from the sum of several smaller scarps, each of which is associated to a single thrust (Fig. 7). The three outer thrusts are clearly visible on the lateral walls of a canyon ~50 m deep carved by a tributary of the Chenab river (Fig. 2B). The shortening absorbed across them make Precambrian limestones overthrust Siwaliks and Quaternary conglomerates. Gouge zones in the limestones and locally fractured conglomerates underline their long-term activity associated to a reverse south-vergent movement. No strike-slip component was observed neither on the fault plane nor at the scale of the geomorphic markers. For these thrusts, we measured *in situ* 30° to 50° north-dipping thrust planes, the dip increasing from the southernmost to the northernmost thrust. For the two southernmost thrusts, which are the only ones clearly reaching the surface, the dip becomes gentler (10–15°N) in the alluvial deposit within the shallower 10–20 m. Considering their relative positions and extrapolating the dips observed on the canyon walls, these thrusts should merge at depth of about 0.5–0.8 km below the surface on a main thrust with an average dip of 45°. The MWT crosscuts obliquely through folded structures located at the back of the FA and is therefore clearly out-of-sequence.

The faulted fan was formed by the Nodda river, a stream essentially draining the limestones in the hanging-wall of the MWT fault zone (Figs. 6 and 7). The fan deposit is entirely stratified with beds 40 to 100 cm thick. These beds are mostly composed of well-sorted sub-angular to angular pebbles with few meter-scale coarser and finer lenses. The maximum thickness of the fan is ~60 m. The upper part of this alluvial formation is consolidated by a carbonate cement, derived from the circulation of fluids in the limestones, producing a calcrete shell that protects the surface against erosion. This preserved marker records the total cumulated deformation since its formation, which coincides with the abandonment of the fan by the vertical incision of Nodda river. Its slope, away from the scarps, progressively decreases from 9 to 6% between the apex and the lower edge of the fan, which are separated by a horizontal distance of 2 km. Assuming that the present slope is the same of the pristine one, before deformation the difference in altitude between the apex and the lower edge of the fan was between 120 m and 180 m. At present, the difference in altitude is 300 m. For the fan surface, we thus estimated a total vertical displacement of 150 ± 30 m across the fault zone.

In absence of quartz-rich units at surface and organic matter in such high-energy deposits, we could not apply the ^{10}Be and ^{14}C dating methods at this site. We thus dated the deposit of the fan with two OSL samples in buried sand units. We collected one sample at shallow depth (JK-10-80, at 6 m depth) at the apex of the fan, and one at the base of the fan (JK-10-33, at 55 m depth) beneath one of the thrusts (Figs. 6 and 7). Both of these samples come from lenses of fine sand, their luminescence signal is therefore likely to have been totally reset during the relatively low-energy fluvial transport from the catchment to the fan (sev-

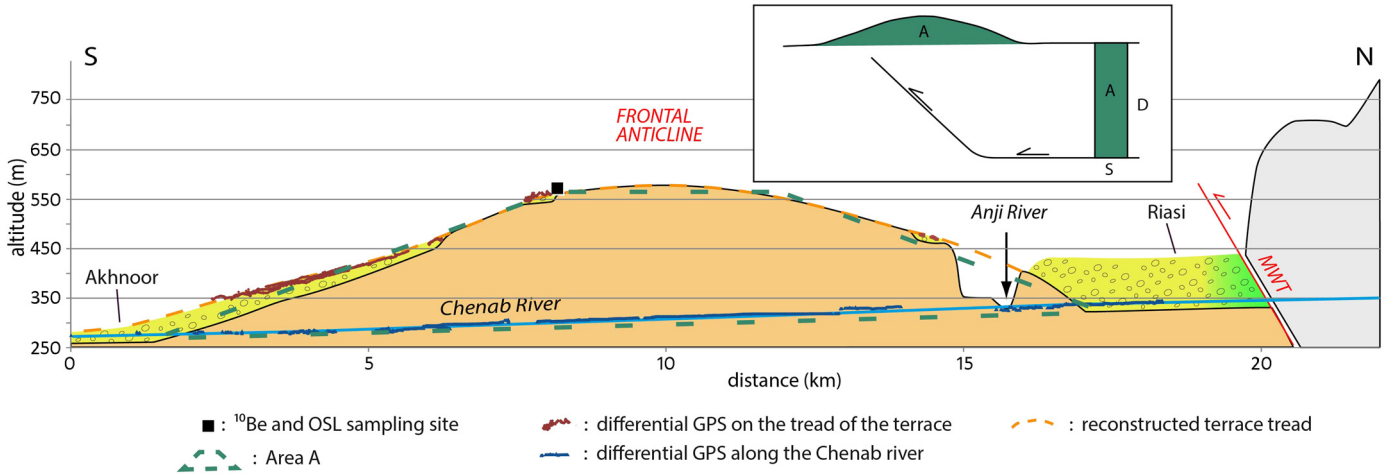

Fig. 8. Cross-section of the FA bounded at the top by a folded strath terrace. Sketch of the method used to calculate the horizontal shortening along the MFT (S) from the area of the fold (A) and the depth of the flat detachment (D) since the abandonment of the terrace.

eral kilometers). The two least burial ages obtained on samples JK-10-80 and JK-10-33 are 15 ± 1 OSL-ka and 14 ± 2 OSL-ka, respectively (Table 1). The overlap of the age intervals for samples at different depths and distances from the outlet suggests that the fan was formed rapidly, in less than a few thousand years. We consider that the youngest age is therefore the closer to the abandonment age, and we assign to the fan surface an age of 14 ± 2 OSL-ka.

Considering the total vertical displacement for the fan surface across the scarps (150 ± 30 m), a mean dip of the faults of 45° (Figs. 2B and 7) and the age of the deformed surface (14 ± 2 ka), the mean slip rate along the MWT is 15.9 ± 5.3 mm/yr. This value corresponds to a NNE–SSW shortening rate of 11.2 ± 3.8 mm/yr, which is more than half of the regional shortening rate measured by geodesy (Schiffman et al., 2013; Jade et al., 2014; Jouanne et al., 2014).

5. The frontal anticline and the Main Frontal Thrust

The FA is perpendicularly crossed by the Chenab river, whose natural section reveals an asymmetrical geometry of the Siwaliks bedding within the two flanks (Fig. 1C). Like the topographic slopes, the bedding in the Northern flank is much steeper than the bedding on the Southern flank and in some places it is even vertical or overturned. This structural geometry may be explained by the presence of a back-thrust at depth. Conformable relief of the anticline suggests a recent enhancement of the folding activity responsible of this "young" topography. The folding is generated by the shortening along the MHT that connects to the ramp of the MFT. This thrust is a blind structure in our study area, as we did not observe any tectonic scarp or rupture at the Southern toes of the FA. Some seismic profiles in the area suggest rooting in the basement beneath complex structures in the core of the anticline (Raiverman et al., 1994; Srinivasan and Khar, 1996).

The width of the FA in the region is 20–25 km, but it reduces to ~15 km in the Chenab reentrant zone between the cities of Riasi and Akhnoor (Fig. 1B). Here, the average N120°E direction of its axis is abruptly deflected with the western part oriented N80°E and the eastern part oriented N160°E. In spite of this sharp variation in direction, the morphology and the geometry at surface of the different Siwaliks units suggest that the FA is a unique structure. Indeed, the front of the anticline is characterized by a linear and continuous break in slope all along the reentrant. This is subparallel to the direction of the stratigraphic limits between the Upper, Middle, and Lower Siwaliks, whose shapes define the geometry at surface of the anticline. The limits between these units, respectively composed of conglomerates, sandstones, and clays, are highlighted by differential erosion and consequent drainage organization. The narrowing of the folded zone in the reentrant is the result of the steepening of the bedding on the two flanks, especially the northern one. This change at surface may be linked to an asperity along the basal décollement (Marshak, 2004) that increases the dip of the ramp at depth and reduces the frontal propagation of the anticline. Therefore, lateral variation of the amount and direction of thrusting may locally occur. Furthermore, this reentrant geometry induces a shortening perpendicular to the convergence direction (Replumaz et al., 2012) and may locally enhance the shortening in the center of the reentrant (Vignon, 2011).

Late Pliocene Mirpur conglomerates (Visser and Johnson, 1978) were deposited in the vicinity of a growing structure suggesting that the FA has been active since at least 2 Ma. Thus, at the geological timescale, the MFT and MWT are simultaneously active. However, in the Late-Quaternary period, the deformation is sometimes – often? – localized on the MWT, implying that out-of-sequence earthquakes occur at the seismic cycle scale.

From the axis of the anticline to the South plain, a large fluvial strath terrace unconformably overlies the deposits of the Siwaliks (Fig. 8). This provides a suitable marker for quantifying the incision of the Chenab river into the anticline. Northward, we correlate the terrace with the remnant of a terrace that was abandoned at the toes of the Northern flank of the anticline, just South of the Anji river. Both remnants are several meters thick, composed of units of sand and decimetric well-rounded cobbles and made of the same lithologies (quartzites, sandstones, traps). The dip of the terrace for the northern remnant is presently a few degrees to the North (i.e. upstream) because of the long-wave folding.

In absence of a well-constrained geometry of the blind ramp at depth, we used the excess area method (Hossack, 1979) and estimated the area of the anticline section under the terrace envelope (A) and the depth of the detachment plane (D) in order to determine a horizontal shortening (S) across this structure since the abandonment of the terrace (Fig. 8). We calculated the area A of 2.3 ± 0.5 km^2 and estimated the depth D of the MHT from the seismic profile of Srinivasan and Khar (1996) at 9 ± 1 km. This yields a horizontal shortening S across the anticline of 212 ± 68 m. To calculate the shortening rate on the MFT over this period this value was divided by the age of the abandonment of the terrace.

We dated the abandonment of the terrace by coupling two geochronometers on the remnant of the terrace at the top of the FA. At this site, on a recently excavated section by the side of a road, we sampled quartzite cobbles along a 1.5-m-vertical profile for ^{10}Be analysis (JK-10-60 to JK-10-65) and collected a sand sample for OSL (JK-10-69) at a depth of 6 m (Table 1). The ^{10}Be

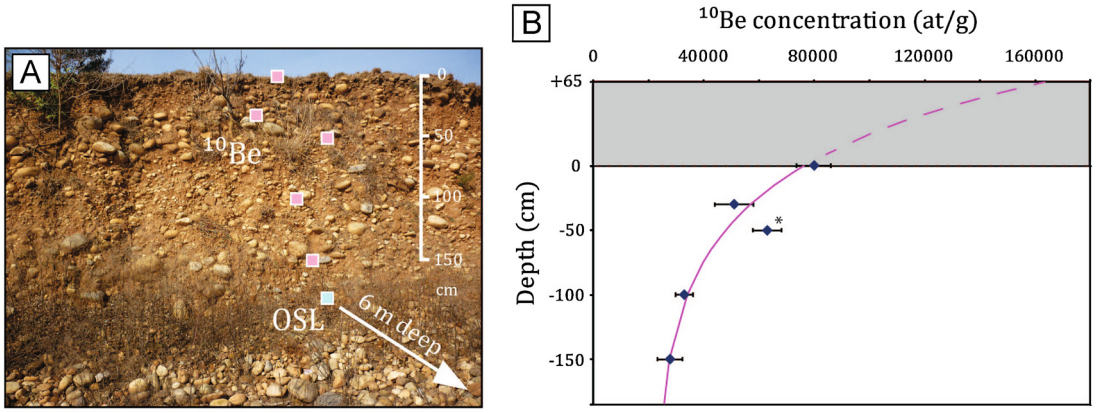

Fig. 9. A) Photograph of the section sampled for ^{10}Be dating within the strath terrace at the top of the FA; B) Plot of the ^{10}Be concentrations versus depth. The solid curve represents the best-fit exponential model of data inversion by least square assuming no denudation, density 2.2 g/cm^3, and particles attenuation values determined by Braucher et al. (2003). The sample with a $*$ was not considered in the inversion. This best-fit model yields an exposure age of 9.6 ka. The dotted part of the curve represents the theoretical concentration for the hypothesis of a ~24 ka age for the terrace (OSL dating) with an instant removal of 65 cm of soil by ploughing.

concentrations, except for sample JK-10-62, show an exponential decrease at depth (Fig. 9). This distribution demonstrates that the sampled profile corresponds to a single depositional event and that it was not disturbed by post-depositional re-mobilization. It also proves that most of the samples are characterized by a common pre-exposure ^{10}Be component. Sample JK-10-62 was considered as an outlier and its concentration may be simply explained by a higher ^{10}Be inherited component. The best-fit model curve ascertained from the least square inversion of the data assuming no denudation (excluding the outlier) tends asymptotically at depth toward a value of $19 \cdot 10^3$ at/g. This quantity is interpreted to be the average inheritance of the samples (see for example Anderson et al., 1996). Subtracting it from the total concentration given by the best fit model at the surface ($77 \cdot 10^3$ at/g), we calculated a minimum exposure age of 9.6 ^{10}Be-ka for this terrace.

However, the top of the profile corresponds to a ploughed field and a few tens of centimeters of soil are likely to have been recently removed from the pristine surface. It means that this minimum ^{10}Be age may underestimate the true exposure age by several thousand years. Such a scenario is consistent with the OSL dating of sample JK-10-69, which yields a least burial age of 24 ± 1 ka and a mean burial age of 34 ± 6 ka. If we consider that the least OSL age is the more representative one, this would imply a recent removal of a thickness of ~65 cm of soil to fit the ^{10}Be best-fit model. Taking into account the consistency between the minimum ^{10}Be exposure age and the least OSL burial age, we assign to this terrace remnant an abandonment age of 24 ± 1 ka.

Since this time, the Chenab river has been vertically incising its riverbed because of the progressive folding as a consequence of the estimated shortening of 212 ± 68 m across the anticline (Fig. 8). This yields a shortening rate over this period of 9.0 ± 3.2 mm/yr accommodated on the MFT. It has to be observed that if we took the minimum ^{10}Be age (9.6 ka), the shortening rate on MFT would be 22.1 ± 7.1 mm/yr, higher than the whole deformation absorbed across the Himalayan range measured by geodesy.

6. Discussion

Our morphotectonic results for the MBT, MWT and MFT show that present deformation in Northwestern Himalaya is localized on the two more external structures. Tectonic activity on the MBT probably ceased more than ~30 ka ago, and we therefore consider that this fault is no longer seismogenic in the region since it would imply very long recurrence period. In contrast, horizontal slip rates on both the MWT (since ~14 ka) and MFT (since ~24 ka) are close to 1 cm/yr. Consequently, at the Late-Quaternary scale, these two thrusts are the main active tectonic structures accommodating a large part of the total India–Eurasia convergence.

The sum of the Late-Quaternary horizontal slip rates on the MWT and MFT, including the uncertainties associated mainly with their geometry at depth, is between 13.2 and 27.2 mm/yr. If we consider the lower bound of these rates, it is within the same range as the instantaneous rate obtained by geodesy (12.5–14 mm/yr). By contrast, if we consider the upper end of these rates, it is significantly larger than the instantaneous rate. We therefore deduce that over the last 15 ka either horizontal rates have been steady, or they recently decreased by as much as 50%. The latter case seems very unlikely considering the steadiness of the convergence rate between India and Eurasia over the geological time scale (e.g. Patriat and Achache, 1984) that is still observed nowadays (e.g. Bettinelli et al., 2006). Furthermore, we may not exclude a locally enhanced shortening rate due to complex geometry at the vicinity of the Chenab reentrant (Marshak, 2004; Vignon, 2011; Replumaz et al., 2012). We therefore believe that lower bounds for the Late-Quaternary rates determined on the MWT and MFT are more realistic.

The regional deformation pattern at the Late-Quaternary time scale is partly in-sequence (slip along the MFT) and partly out-of-sequence (slip along the MWT). Indeed, earthquakes associated with this deformation may be either localized on one of the two ramps or on the main common basal detachment. In the first case, seismogenic ruptures propagate along structures a few kilometers long lying between the base of the ramp and the surface (for the MWT) or the sub-surface (for the MFT) as observed for the 2005 Muzaffarabad Mw 7.6 earthquake (Yan et al., 2013). In the second case, large seismogenic ruptures may propagate over several tens of kilometers of the sub-flat MHT before reaching one or both ramps.

If we consider that the brittle/ductile transition on the MHT is situated at the level of the ramp that uplifts the Pir Panjal range (Fig. 1), the length of the seismogenic structures would be around 60 km for the MWT + MHT and 75 km for MFT + MHT. The potential breaking area on these faults lying between the surface rupture of the 2005 Muzaffarabad earthquake to the West and the presumed surface rupture of the 1905 Kangra earthquake to the East (~200 km) is therefore ~12 000 km^2 in the first case and ~15 000 km^2 in the second. If all the seismic gap zone is affected by a single rupture, for an average co-seismic slip of ~4 m like the Muzaffarabad event (Avouac et al., 2006), a total rupture of the MHT and either of the two ramps in this zone could generate a Mw 8.1–8.2 earthquake (Kanamori, 1983). For a total release of the

slip deficit accumulated since 1555 at ~13 mm/yr, the co-seismic slip would be ~6 m and would produce a Mw 8.2–8.3 earthquake.

The limits of the seismogenic zone need to be better constrained through thermo-mechanical studies at the crustal scale. However, here we have shown: 1) high fault slip rates in the order of 1–2 cm/yr; 2) several meters of elastic deformation not seismically released since at least the last major regional event in 1555; 3) structures whose geometry is compatible with the occurrence of Mw > 8 earthquakes.

7. Conclusion

This study shows that deformation in the Northwestern Himalayan during the Late-Quaternary follows an in-sequence/out-of-sequence pattern. Two main regional seismogenic structures, the Medlicott–Wadia Thrust and the Main Frontal Thrust, accommodate most of the shortening across the Himalayan belt. These thrusts connect at depth on a main basal detachment located within the Paleozoic basement, the Main Himalayan Thrust, and where the reverse movement responsible for the mountain building is concentrated. We have quantified the shortening rate at 11.2 ± 3.8 mm/yr over the last ~14 ka for the Medlicott–Wadia Thrust and at 9.0 ± 3.2 mm/yr over the last ~24 ka for the Main Frontal Thrust. This implies a total Late-Quaternary shortening rate for the Main Himalayan Thrust between 13.2 and 27.2 mm/yr, the lower bound of this range being consistent with geodetic rates.

We can therefore expect earthquakes that break structures both at the very front of the range or in a more internal position. To better constrain the seismic hazard in this densely populated region, paleoseismological studies are necessary to determine whether all the accumulated slip deficit is seismically released and to know which segments have already broken together. In parallel, thermo-mechanical modeling of the potential surface rupture on the main detachment is fundamental to better constrain the maximal magnitude expected along this part of the Himalayan front.

Acknowledgements

This research was funded by the PAKSIS program of the ANR Catel, INSU TS-ALEAS, and Labex@OSUG 2020. We thank Jammu and Kashmir inhabitants for their help in the fieldwork and their witness statements about earthquakes felt. We thank Maurice Arnold, Georges Aumaître and Karim Keddadouche for assistance during AMS measurements for Beryllium 10. RJ conducted this work under the collaborative grant from the WIHG Project and MoES Project vide # MoES/P.O (Geosci)/11/2013, Govt. of India. RJ and PS kindly extend acknowledgment for the Director, WIHG, DDN for providing necessary support for this collaboration. The manuscript was considerably improved thanks to fruitful and detailed comments from T. Berthet and 2 other anonymous reviewers. We finally thank Daria Zandomeneghi for English editing.

Appendix A. Supplementary material

Supplementary material related to this article can be found online at http://dx.doi.org/10.1016/j.epsl.2014.11.030.

References

Ambraseys, N.N., Jackson, D., 2003. A Note on Early Earthquakes in Northern India and Southern Tibet, Bangalore. INDE, Current Science Association. 13 p.

Ambraseys, N.N., Douglas, J., 2004. Magnitude calibration of north Indian earthquakes. Geophys. J. Int. 159, 165–206.

Anderson, R.S., Repka, J.L., Dick, G.S., 1996. Explicit treatment of inheritance in dating depositional surfaces using in situ ^{10}Be and ^{26}Al. Geology 24, 47–51.

Avouac, J.-P., Ayoub, F., Leprince, S., Konca, O., Helmberger, D.V., 2006. The 2005, Mw 7.6 Kashmir earthquake: sub-pixel correlation of ASTER images and seismic waveforms analysis. Earth Planet. Sci. Lett. 249, 514–528.

Balco, G., Stone, J.O., Lifton, N.A., Dunai, T.J., 2008. A complete and easily accessible means of calculating surface exposure ages or erosion rates from ^{10}Be and ^{26}Al measurements. Quat. Geochronol. 3, 174–195.

Bettinelli, P., Avouac, J.-P., Flouzat, M., Jouanne, F., Bollinger, L., Willis, P., Chitrakar, G., 2006. Plate motion of India and interseismic strain in the Nepal Himalaya from GPS and DORIS measurements. J. Geod. 80, 567–589.

Bilham, R., 2001. Slow tilt reversal of the Lesser Himalaya between 1862 and 1992 at 78°E, and bounds to the southeast rupture of the 1905 Kangra earthquake. Geophys. J. Int. 144, 713–728.

Braucher, R., Brown, E.T., Bourlès, D.L., Colin, F., 2003. In situ produced ^{10}Be measurements at great depths: implications for production rates by fast muons. Earth Planet. Sci. Lett. 211, 251–258.

Burbank, D.W., Johnson, G.D., 1983. The late Cenozoic chronologic and stratigraphic development of the Kashmir intermontane basin, Northwestern Himalaya. Palaeogeogr. Palaeoclimatol. Palaeoecol. 43, 205–235.

Burbank, D.W., Raynolds, R.G.H., Johnson, G.D., 1986. Late Cenozoic tectonics and sedimentation in the north-western Himalayan foredeep, II, Eastern limb of the northwest syntaxis and regional synthesis. In: Spec. Publ. Int. Assoc. Sedimentol., vol. 8, pp. 293–306.

Chmeleff, J., von Blanckenburg, F., Kossert, K., Jakob, J., 2010. Determination of the ^{10}Be half-life by multicollector ICP-MS and liquid scintillation counting. Nucl. Instrum. Methods Phys. Res., Sect. B 268 (2), 192–199.

Dunne, J., Elmore, D., Muzikar, P., 1999. Scaling factors for the rates of production of cosmogenic nuclides for geometric shielding and attenuation at depth on sloped surfaces. Geomorphology 27, 3–11.

Fuchs, G., 1975. Contributions to the geology of the northwestern Himalayas. Abh. Geol. Bundesanst. 32, 3–59.

Gansser, A., 1964. Geology of the Himalayas. InterScience Publishers, John Wiley & Sons. 289 p.

Hebeler, A., Madden, C., Malik, M.A., Kaericher, M., Gavillot, Y., Yule, D., Meigs, A., 2010. Middle Holocene surface rupture of the Riasi thrust, Kashmir, India. In: Annual Meeting of the Seismological Society of America. Portland, OR, 21–23 April 2010.

Hossack, J.R., 1979. The use of balanced cross-sections in the calculation of orogenic contraction: a review. J. Geol. Soc. 136, 705–711. http://dx.doi.org/10.1144/gsjgs.136.6.0705.

Hussain, A., Yeats, R., MonaLisa, 2009. Geological setting of the 8 October 2005 Kashmir earthquake. J. Seismol. 13, 315–325.

Jade, S., Mukul, M., Gaur, V.K., Kumar, K., Shrungeshwar, T.S., Satyal, G.S., Dumka, R.K., Jagannathan, S., Ananda, M.B., Kumar, P.D., Banerjee, S., 2014. Contemporary deformation in the Kashmir–Himachal, Garhwal and Kumaon Himalaya: significant insights from 1995–2008 GPS time series. J. Geod. 88, 539–557. http://dx.doi.org/10.1007/s00190-014-0702-3.

Jouanne, F., Awan, A., Madji, A., Pêcher, A., Latif, M., Kausar, A., Mugnier, J.L., Khan, I., Khan, N.A., 2011. Postseismic deformation in Pakistan after the 8 October 2005 earthquake: evidence of afterslip along a flat north of the Balakot–Bagh thrust. J. Geophys. Res. 116, B07401.

Jouanne, F., Awan, A., Pêcher, A., Kausar, A., Mugnier, J.L., Khan, I., Khan, N.A., Van Melle, J., 2014. Present-day deformation of northern Pakistan from Salt Ranges to Karakorum Ranges. J. Geophys. Res., Solid Earth. http://dx.doi.org/10.1002/2013JB010776.

Kanamori, H., 1983. Magnitude scale and quantification of earthquakes. Tectonophysics 93, 185–199.

Kaneda, H., Nakata, T., Tsutsumi, H., Kondo, H., Sugito, N., Awata, Y., Akhtar, S.S., Majid, A., Khattak, W., Awan, A.A., Yeats, R.S., Hussain, A., Ashraf, M., Wesnousky, S.G., Kausar, A.B., 2008. Surface rupture of the 2005 Kashmir, Pakistan, earthquake and its active tectonic implications. Bull. Seismol. Soc. Am. 98, 521–557.

Karunakaran, C., Rao, R.A., 1979. Status of exploration for hydrocarbons in Himalayan Region – contribution to stratigraphy and structure. Misc. Pub. Geol. Sur. Ind. 41, 1–66.

Korschinek, G., Bergmaier, A., Faestermann, T., Gerstmann, U.C., Knie, K., Rugel, G., Wallner, A., Dillmann, I., Dollinger, G., von Gostomski Lierse, Ch., Kossert, K., Maitia, M., Poutivtsev, M., Remmert, A., 2009. A new value for the half-life of ^{10}Be by heavy-ion elastic recoil detection and liquid scintillation counting. Nucl. Instrum. Methods Phys. Res., Sect. B 268 (2), 187–191.

Krishnaswamy, V.S., Jalote, S.P., Shome, S.K., 1970. Recent crustal movements in north-west Himalaya and the Gangetic foredeep and related patterns of seismicity. In: 4th Symp. Earthquake Eng., Roorkee, pp. 419–439.

Kumahara, Y., Nakata, T., 2006. Active Faults in the Epicentral Area of the 2005 Pakistan Earthquake. In: Spec. Publ., vol. 41. Res. Cent. Reg. Geogr. Hiroshima Univ., p. 54.

Lal, D., 1991. Cosmic ray labeling of erosion surfaces: in situ nuclide production rates and erosion models. Earth Planet. Sci. Lett. 104, 424–439.

Marshak, S., 2004. Salients, recesses, arcs, oroclines, and syntaxes; a review of ideas concerning the formation of mapview curves in fold-thrust belts. In: McClay, K.R. (Ed.), Thrust Tectonics and Hydrocarbon System. In: AAPG Mem., vol. 82, pp. 131–156.

Mugnier, J.L., Gajurel, A., Huyghe, P., Jayangondaperumal, R., Jouanne, F., Upreti, B., 2013. Structural interpretation of the great earthquakes of the last millennium in Central Himalaya. Earth-Sci. Rev. 127, 30–47.

Murray, A.S., Wintle, A.G., 2000. Luminescence dating of quartz using an improved single-aliquot regenerative-dose protocol. Radiat. Meas. 32, 57–73.
Nakata, T., Tsutsumi, H., Khan, S., Lawrence, R., 1991. Active faults of Pakistan. In: Spec. Publ., vol. 21. Res. Cent. Reg. Geogr. Hiroshima Univ.. 141 p.
Nawani, P.C., Khan, S.A., Singh, O.R., 1982. Geologicum geomorphic evolution of the western part of Chenab basin with special reference to Quaternary tectonics. Himal. Geol. 12, 18.
Ni, J., Barazangi, M., 1984. Seismotectonics of the Himalayan Collision Zone, geometry of the underthrusting Indian Plate beneath the Himalaya. J. Geophys. Res. 89, 1147–1163.
Patriat, P., Achache, J., 1984. India–Eurasia collision chronology has implications for crustal shortening and driving mechanism of plates. Nature 311, 615–621. http://dx.doi.org/10.1038/311615a0.
Pêcher, A., Seeber, L., Guillot, S., Jouanne, F., Kausar, A., Latif, M., Majid, A., Mahéo, G., Mugnier, J.L., Rolland, Y., van der Beek, P., Van Melle, J., 2008. Stress field evolution in the northwest Himalayan syntaxis, northern Pakistan. Tectonics 27, TC6005.
Powers, P.M., Lillie, R.J., Yeats, R.S., 1998. Structure and shortening of the Kangra and Dehra Dun reentrants, Sub-Himalaya, India. Geol. Soc. Am. Bull. 110, 1010–1027.
Raiverman, V., Srivastava, A.K., Prasad, D.N., 1994. Structural style in northwestern Himalayan foothills. Himal. Geol. 15, 263–280.
Ramsey, C.B., 1995. Radiocarbon Calibration and Analysis of Stratigraphy: the OxCal Program. ETATS-UNIS, University of Arizona, Tucson, AZ. 795 p.
Replumaz, A., Vignon, V., Regard, V., Martinod, J., Guerrero, N., 2012. East–west shortening during north–south convergence, example of the NW Himalayan syntaxis. Aust. J. Earth Sci. 59, 1–14.
Schiffman, C., Bali, B.S., Szeliga, W., Bilham, R., 2013. Seismic slip deficit in the Kashmir Himalaya from GPS observations. Geophys. Res. Lett. 40, 5642–5645. http://dx.doi.org/10.1002/2013GL057700.
Seeber, L., Armbruster, J.G., 1984. Some elements of continental subduction along the Himalayan front. Tectonophysics 105, 263–278.
Srinivasan, S., Khar, B.M., 1996. Status of hydrocarbon exploration in Northwest Himalaya and foredeep – contribution to stratigraphy and structure. In: Geol. Surv. India Spec. Publ., vol. 21, pp. 295–405.
Srivastava, P., Tripathi, J., Islam, R., Jaiswal, M.K., 2008. Fashion and phases of late Pleistocene aggradation and incision in the Alaknanda River Valley, western Himalaya, India. Quat. Res. 70, 68–80.
Stone, J.O., 2000. Air pressure and cosmogenic isotope production. J. Geophys. Res. 105, 23753–23759.
Thakur, V.C., Jayangondaperumal, R., Malik, M.A., 2010. Redefining Medlicott-Wadia's main boundary fault from Jhelum to Yamuna, an active fault strand of the main boundary thrust in northwest Himalaya. Tectonophysics 489, 29–42.
Vignon, V., 2011. Activité hors séquence des chevauchements dans la syntaxe nord-ouest himalayenne: apports de la modélisation analogique et quantification quaternaire par analyse morphotectonique. PhD thesis. Université de Grenoble, France. 278 p.
Visser, C.F., Johnson, G.D., 1978. Tectonic control of Late Pliocene molasse sedimentation in a portion of the Jhelum Re-Entrant, Pakistan. Geol. Rundsch. 67 (1), 15–87.
Wallace, K., Bilham, R., Blume, F., Gaur, V.K., Gahalaut, V., 2005. Surface deformation in the region of the 1905 Kangra Mw = 7.8 earthquake in the period 1846–2001. Geophys. Res. Lett. 32, L15307. http://dx.doi.org/10.1029/2005GL022906.
Wesnousky, S.G., Kumar, S., Mohindra, R., Thakur, V.C., 1999. Uplift and convergence along the Himalayan Frontal Thrust of India. Tectonics 18, 967–976.
Yan, Y., Pinel, V., Trouvé, E., Pathier, E., Perrin, J., Bascou, P., Jouanne, F., 2013. Coseismic slip distribution of the 2005 Kashmir earthquake from SAR amplitude image correlation and differential interferometry. Geophys. J. Int.. http://dx.doi.org/10.1093/gji/ggs102.
Yeats, R.S., Kausar, A., Nakata, T., 2006. Conferees examine deadly 2005 Kashmir Earthquake. Eos 87, 115.
Yin, A., 2006. Cenozoic tectonic evolution of the Himalayan orogen as constrained by along-strike variation of structural geometry, exhumation history, and foreland sedimentation. Earth-Sci. Rev. 76, 1–131.